Particle Kinetics and Dynamics in Flaring Atmospheres Leading to Sunquakes

Particle Kinetics and Dynamics in Flaring Atmospheres Leading to Sunquakes

By

Valentina Zharkova and Serhii Zharkov

Cambridge
Scholars
Publishing

Particle Kinetics and Dynamics in Flaring Atmospheres Leading to Sunquakes

By Valentina Zharkova and Serhii Zharkov

This book first published 2025

Cambridge Scholars Publishing

Lady Stephenson Library, Newcastle upon Tyne, NE6 2PA, UK

British Library Cataloguing in Publication Data
A catalogue record for this book is available from the British Library

ISBN: 978-1-0364-5856-0
ISBN (Ebook): 978-1-0364-5857-7

Contents

1
The observational constraints in solar flares and interplanetary space

Energetic particles play a significant role in energy transfer inside the Sun and from the Sun to interplanetary space and planetary atmospheres. Solar energetic particles (SEP) are often associated with solar flares, streaming into the solar atmospheres and towards the interplanetary space. There are also energetic particles of solar wind originally generated from the Sun, which can undergo additional acceleration in current sheets formed in the interplanetary space. The nature of their energisation and transport over the solar atmosphere or interplanetary space are important in understanding the processes governing the solar-terrestrial connection.

1.1 Solar flares

The complex processes of plasma heating in solar flares are associated with a primary release of magnetic energy via magnetic reconnection occurring in the corona [Priest and Forbes 2000a, Somov 2000] and subsequent acceleration of energetic particles [Vilmer et al. 2011, Zharkova et al. 2011a] precipitating along newly reconnected field lines [Holman et al. 2011, Kontar et al. 2011]. These processes happen within a very short timescale during flare onset and can be effectively diagnosed from the increase of intensities in flaring emission of hard X-rays (HXR), γ-ray (GR), soft X-rays (SXR), extreme ultra-violet (EUV), ultra-violet (UV) and optical emission [Matthews et al. 2015, and references therein].

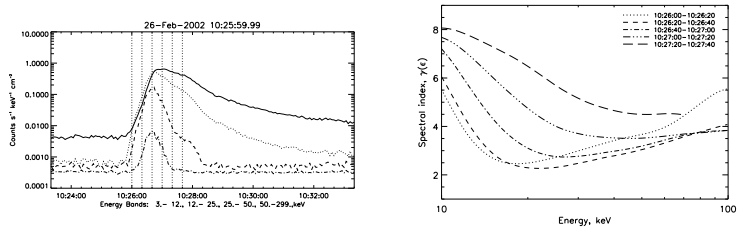

Fig. 1.1: Upper Panel: Temporal variation (4-second cadence) of the count rates in seven front RHESSI segments for the 2002, February26 solar flare (10:26 UT). The vertical lines show five 20-second accumulation intervals for spectral analysis. Lower Pane: Temporal variation of the energy-dependent photon spectral index $\gamma(\epsilon) = -d\log I(\epsilon)/d\log\epsilon$. Each line corresponds to one time interval. From Kontar and MacKinnon [2005].

Energetic electron beams precipitating into the flaring atmosphere [Brown 1971, Syrovatskii and Shmeleva 1972a;b] can account for HXR and MW emission [Holman et al. 2011, Kontar et al. 2011] while proton and ion beams [Vilmer et al. 2011] can account for observed γ-ray emission. The scenarios by which the magnetic field is reconfigured while triggering flaring events and converting the energy of magnetic field into radiation and macro-motions in flares are to a large extent defined by the initial magnetic field topologies of interacting loops and the trigger mechanisms that initiate the reconnection process in each flaring case [Priest and Forbes 2000a, Somov 2000].

1.1.1 Summary of HXR and SXR emission features

1.1.1.1 Lightcurves

Spatially-integrated hard X-ray lightcurves obtained by RHESSI or STIX payload shown as example in Fig.1.1, top plot, done for the flare of the 26 February, 2002, showing sharp increases (bursts) of hard X-ray intensity over a relatively short ($\sim$ 0.5 – 5 seconds) timescale accompanied by a more slowly varying

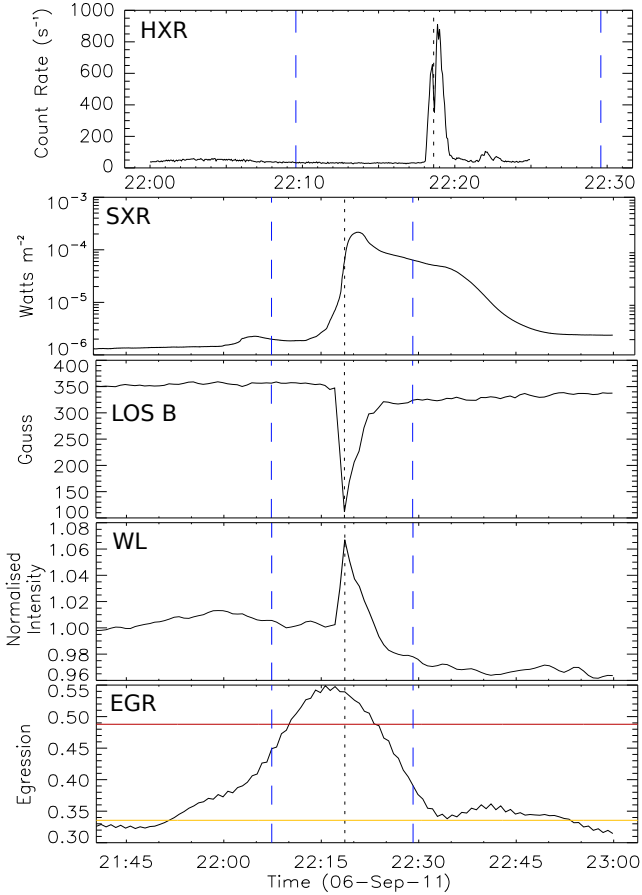

Fig. 1.2: Light curves for the flare of 6 September 2011 of RHESSI $100 - 300keV$ HXR (HXR), GOES ($1.0 - 8.0$Å) SXR (SXR), integrated HMI LOS magnetogram (LOS B), WL continuum (WL) and egression power (EGR). The HMI data products are integrated over the seismic signal. Black vertical dotted line denotes the sunquake onset time (22:18:37 UT) from time-distance diagrams (see chapter 12). Continuum emission shows a peak emission at 22:18:37 UT, coincident with quake onset and LOS magnetogram transient. Egression power, normalised with respect to quiet sun levels, peaks above a defined detection threshold (red horizontal line) of the local mean (yellow) plus 5σ within the flare temporal window (blue vertical lines). A courtesy of Macrae et al. [2018].

component with a timescale up to a few tens of minutes. The appearance of both sharp hard X-ray (HXR) bursts and steady increases in hard X-ray intensity suggest that electrons are accelerated on two fundamentally distinct timescales: a rapid acceleration to high, bremsstrahlung-emitting energies and a more stationary process that maintains the high-energy electron flux to produce steady hard X-ray emission for a substantial fraction of an hour or even longer.

At lower photon energies ϵ, where thermal bremsstrahlung dominates the total emission, the emission at higher photon energies is weighted more heavily by plasma at high temperatures T. As a result, the decrease in conductive cooling time with temperature ($\tau \sim T^{-5/2}$) leads to the emission at higher energies peaking sooner [Aschwanden 2007], and hence the lightcurve peaking progressively earlier with increase in photon energy. At higher energies, where non-thermal bremsstrahlung dominates, the relative timing of the emission at different energies depends on both the the reduced "time-of-flight" for higher energy electrons before they impact upon the thick target of the lower atmosphere [which tends to advance high energy emissions relative to low energy ones – Aschwanden and Schwartz 1996, Brown et al. 1998] and on the decrease in collision frequency with energy [which tends to delay high energy emissions relative to low energy ones – Aschwanden et al. 1997]. Hard X-ray emission during flares typically shows a very steep spectrum at lower energies $\epsilon \sim 10$ keV, indicative of a thermal process. Although, the assumption of an isothermal source can be inconsistent with the observations of temporal variations of the hard X-ray spectrum in flares observed by RHESSI and now by STIX [Aschwanden 2007].

These spikes of HXR emission shown in Fig.1.2, top plot, for the flare of the 6 September 2011 are often followed by the increases of other high energy emission - soft X-ray (SXR), ultraviolet (UV) and extra UV (EUV) etc. SXR emission (see Fig.1.2, 2nd plot), transient variations of magnetic field (3rd plot) discussed in section 1.1.2, increase of white light emission (4th plot) and seismic egression power (bottom plot). SXR emission is assumed to be caused by the ambient plasma heating by particle beams produces emission in highly ionised elements, including e.g. Fe XXIV and Fe XXV ions [Porquet et al. 2001, Kawate et al. 2016c, Kuhar et al. 2016], and often shows a longer (hours) duration. Furthermore, there are observed blue-shifts in SXR and EUV emission with upward velocities of up to thousand km$\cdot$s^{-1} [Antonucci et al. 1982,

Milligan et al. 2006a;b, Del Zanna 2008, Milligan and Dennis 2009, Polito et al. 2016]. In addition, observations of Lyman-α lines by the instruments with low spatial resolution show impulsive brightening of Lyman line emission and the appearance of either red or blue wing asymmetries at different times of flare developments [Druett and Zharkova 2018, Dominique et al. 2018]. This is also supported by brightening in Lyman continuum intensity, which becomes greatly enhanced in the head, resulting in strong flattening over the continuum wavelengths [Machado et al. 2018, Druett and Zharkova 2019].

1.1.1.2 Hard X-ray footpoint and coronal sources

The imaging capabilities of RHESSI, combined with its high spectral resolution, have allowed us to resolve in detail coronal sources [e.g., Masuda et al. 1994] and footpoints occurring in the same flare. See, for example, Figure 1.3 demonstrating the coronal and two footpoint sources in the flare of 23 July 2002 [Zharkova et al. 2005b]). This indicates a need to study the acceleration processes in flares that give rise to such different HXR sources.

The coronal source often appears before the main flare hard X-ray increase and the appearance of footpoints . In the impulsive phase, the coronal hard X-ray emission is, generally, well correlated in both time and spectrum with the footpoints [Emslie et al. 2003, Battaglia and Benz 2006]. These observations suggest strong coupling between the corona and chromosphere during flares, a coupling that is presumably related to transport of accelerated particles from one region to the other.

1.1.1.3 Hard X-ray and gamma-ray source geometry

Simultaneous hard X-ray and Gamma-ray images were first observed by RHESSI for the flare of 2002, July 23, as shown in Fig.1.4 [Hurford et al. 2003]. It has been established that the hard X-ray sources in this flare are spatially separated by several arcseconds from the 2.223 MeV neutron-capture Gamma-ray source. A similar, but smaller, separation was also detected for the "Halloween" flare of 2003, October 28 [Hurford et al. 2006].

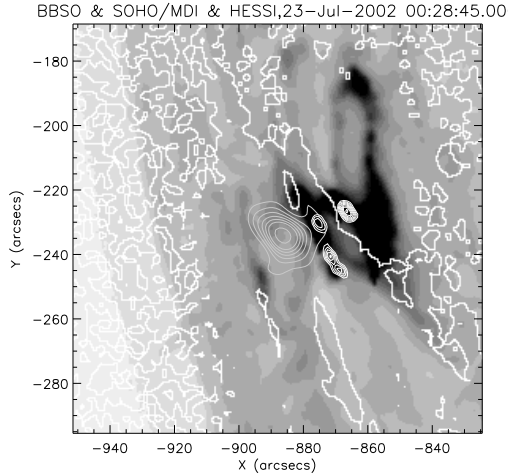

Fig. 1.3: RHESSI hard X-ray images of the flare of 2003, July 23, (white thin contours) taken at 00:28 UT, overlaid on the MDI neutral-line magnetograms (white thick contours) and Hα images (negatives) taken at 00:28:45 UT. One extended (coronal A) and three compact (footpoint, B,C and D) hard X-ray sources are evident. From Zharkova et al. [2005b].

1.1.2 Magnetic Field Changes Associated with Flares

In Fig.1.5 there is an cartoon demonstrating the interaction of magnetic loops A and B appearing on the solar surface from beneath the existing magnetic loop C, which create two places marked as numbers 1 and 2 where the new loops touch the existing one and create reconnecting current sheets 1 and 2. These current sheets initiate the flare onset and generate energetic particles precipitating both downwards along the magnetic loops, creating all the multi-wavelength emission in HXR, SXR, UV, optical rage seen from flares and upwards towards the interplanetary space and planets of solar system as solar energetic particles (SEPs).

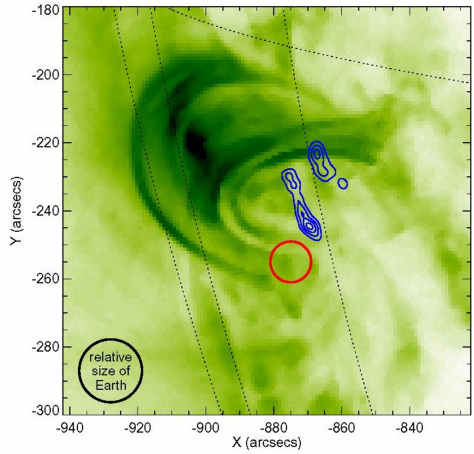

Fig. 1.4: The distant locations of HXR (blue lines) and γ-ray (red line) sources for the flare of 23 July 2003. Courtesy of Lin et al. [2003a].

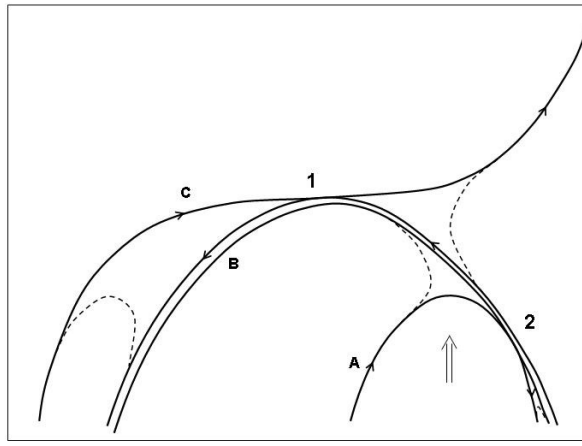

Fig. 1.5: Schematic drawings illustrating the presence of two simultaneous reconnection sites (labeled 1 and 2) in a flare. Loop system A is the main driver, and reconnection 1 is the main energy release site. Reconnected field lines are indicated by dashed curves (from Benz et al., 2005).

1.1.2.1 Overall topological magnetic field changes

The sharp temporal increases of hard X-ray emission are often closely correlated in time with the variations of a magnetic field measured on the photosphere [Kosovichev and Zharkova 2001, Sudol and Harvey 2005, Zharkova et al. 2005b]. For the flare of 2002 July 23, the magnetic flux change over the flare duration was about 1.2×10^{21} Mx; note that the magnetic flux in the areas not spanned by the magnetic inversion line do not show significant variations above the noise level (see Fig.1.6). The magnetic field changes occurring in around apparent magnetic neutral line (AMNL), in general, (see Fig.1.6) and in the locations of 3 HXR footpoint sources of the flare of 23 July 2002 [see Fig. 9 in Zharkova et al. 2005b] are irreversible, or step-like , e.g. the magnetic field reaches a new level of the steady state and does not return to a pre-flare

value [Kosovichev and Zharkova 2001, Sudol and Harvey 2005, Zharkova et al. 2005b].

The magnetic flux in the other areas of either positive or negative polarities, not including the magnetic inversion line, does not show noticeable variations above the noise level. A cross-correlation analysis with a time lag between the temporal magnetic variations of AMNL and the hard X-ray light curves, for the 23 July 2002 flare, reveals a noticeable positive correlation of 0.5-0.6, with the time lag being not bigger than 1-2 minute for all energy bands (see Fig.1.7). This observation strengthens the belief, on the theoretical grounds, that the irreversible changes in the magnetic field are responsible for the initiation and development of flare phenomena.

1.1.2.2 Local magnetic field variations

tIn order to detect magnetic field variations in the locations of HXR emission, the precise RHESSI hard X-ray images in the 40-80 KeV band with the four hard X-ray sources appearing during the course of the flare were overlaid onto the MDI magnetograms [Zharkova et al. 2005b]. The magnetic flux variations were extracted from the maximum areas covered by this hard X-ray emission for each minute before and after the flare onset for four hard X-ray sources (A,B,C,D) detected in the flare of 23 July 2002 (see Fig.1.8).

The source A is found not to be associated with any magnetic field changes, despite it appears in 12-25 KeV band 1 minute earlier than the other footpoint sources B, C and D, but still 1 minute later after a start of the magnetic changes. The source A is likely a projection of the top of the loop (see the TRACE image overlaid onto the H_α-image, Fig.1.3, the loop is embedded into the photosphere at the locations close to the footpoints (sources B, C and D, see section 1.1.1.2). The source A can be a good candidate for the site of primary electron acceleration in the corona because of the hard X-ray emission timing, energy and its relation with the radio emission discussed by Lin et al. [2003a], Krucker et al. [2003]. However, it does not show direct connections with the magnetic field locations, possibly, because of its occurrence on the loop's top and the loop tilt towards the limb.

The temporal variations of magnetic field in the footpoint sources B, C and D are presented in Fig. 1.8 (from the bottom to the top, respectively). The sources

B, C and D are clearly the footpoint locations and, hence, their connection with the magnetic field changes are much more pronounced. The changes in footpoints B and D are fully irreversible, the magnetic field in them decreases from -300 to -420 G, the source D has these changes from 00:26:00 UT for 2 minutes, which are followed at 00:29:00 UT by the magnetic changes in the sources B and C lasting for 2 and 4 minutes, respectively.

In the source C the magnetic changes are mostly reversible with the magnetic field first decreases from 400 G to 100 G and returns to about 300 G after the flare (Fig.1.8, bottom). Since in the source C a difference between the new level of magnetic field, achieved after any changes were stopped, and the pre-flare level is close to the magnitude of irreversible changes measured in the footpoints B and D, we can conclude that these changes are partially irreversible. The major part of these magnetic variations in the source C are reversible of the transient type, which are not real magnetic field changes but those caused by an short-term increase of the line intensity caused by the non-thermal excitation by by precipitating high-energy electrons of the upper level of the Ni atom in the transition 6768 A where the magnetic field is measured [see for details Zharkova and Kobylinskii 1993, Zharkova and Kosovichev 2002].

1.1.2.3 Morphology of the active region NOAA 11283

This schematic example of magnetic topology in flares shown in Fig.1.5 is demonstrated in active region (AR) NOAA 11283 which produced two X-class flares on September 6 and 7, 2011 showing the observed magnetic field changes [Liu et al. 2014a, Petrie 2016, Macrae et al. 2018] and flare energetics [Feng et al. 2013]. The X2.1 class flare occurred on September 6, 2011 produced ripples reflecting seismic response to the flare, shortly called a sunquake [Kosovichev and Zharkova 1998, Macrae et al. 2018].

The X2.1 flare starts with the activation of an S-shaped sigmoid, representing a flux rope, seen in the 94 ÅAIA data (Fig.1.9, left plot)). During the flare onset (22:18:37 UT) there are observed two flaring loops and circular Hα ribbon (Fig.1.9, right plot [Macrae et al. 2018]. NOAA 11283 undergoes a period of flux emergence prior to the September 6 2011 flare, leading to a fan-spine reconnection initiating the flare [Jiang et al. 2014]. This process leads to repeated eruptions with a stronger eruption to the south at 22:19 UT, followed by ribbons